Journal of
Polymer Materials

Tech Science Press

https://doi.org/10.32604/jpm.2026.076443

ARTICLE

Reactive Integration of Amino-Functional 9,10-Dihydro-9-oxa-10-phosphaphenanthrene-10-oxide (DOPO)-modified metal–organic frameworks (MOFs) into Polyurea Balancing Flame Retardancy and Mechanical Properties

Yifan Wang[1], Xishun Qiu[1], Chao Wu[1], Jiazhao Li[1], Chang Dai[1], Bowen Han[1], Jinhu Hu[2], Mingliang Ma[1,*] and Ye-Tang Pan[2,*]

[1]School of Civil Engineering, Qingdao University of Technology, Qingdao, China
[2]National Engineering Research Center of Flame Retardant Materials, School of Materials Science & Engineering, Beijing Institute of Technology, Beijing, China

*Corresponding Authors: Mingliang Ma. Email: mamingliang@qut.edu.cn; Ye-Tang Pan. Email: pyt@bit.edu.cn

Received: 20 November 2025; Accepted: 04 February 2026; Published: 03 April 2026

ABSTRACT: Polyurea (PUA) is widely valued in protective coatings and structural reinforcement because of its impressive mechanical strength and resistance to corrosion. Its high flammability, together with the poor dispersion that often comes with simply blending in flame retardants, continues to limit its use in demanding environments. To overcome these issues, this study introduces a different approach. We grafted 9,10-dihydro-9-oxa-10-phosphaphenanthrene-10-oxide (DOPO) onto the surface of a metal–organic framework (MOF) and then partially amino-functionalized the DOPO layer, ultimately creating an amino-modified DOPO–MOF hybrid. The introduced amino groups can directly react with the isocyanate (–NCO) groups in the PUA matrix, allowing the flame-retardant component to be integrated via reactive integration rather than physical blending. This approach helps avoid the interfacial defects and the mechanical weakening typically observed in conventional blending. With 5 wt% ZIF-67@DOPO-NH_2 added to the PUA system, the composite successfully reached a UL-94 V-0 classification and showed a notable increase in limiting oxygen index (LOI), from 19.2% to 23.8%. The peak heat release rate and total heat release dropped by 36.3% and 38.7%, respectively. Meanwhile, the tensile strength decreased from 25.74 to 22.52 MPa, while the elongation at break remained above 300%, indicating that the material maintained excellent toughness.

KEYWORDS: PUA; DOPO; MOFs; flame retardancy; mechanical properties

1 Introduction

PUA has long found its place in a wide range of applications, from protective coatings and structural strengthening to military-grade protective systems, largely because of its impressive resistance to chemical corrosion, remarkable abrasion durability, fast-curing behavior, and overall ease of use [1–5]. These advantages come with a serious drawback. PUA, as an organic polymer, is inherently highly flammable. Once ignited, the flames race across its surface, and the material releases thick smoke accompanied by toxic gases, an alarming combination that raises substantial safety concerns. Such fire-related vulnerabilities severely restrict PUA's deployment in advanced, performance-critical sectors where reliability under extreme conditions is non-negotiable. For this reason, the quest to develop flame-retardant strategies capable of

curbing PUA's combustibility and improving its safety profile has become not merely important, but an urgent scientific and engineering challenge that demands immediate attention [6–8].

With the growing push toward halogen-free flame-retardant technologies, phosphorus-based systems have come to the forefront, valued for their strong flame-retardant efficiency and their comparatively low environmental impact. Among them, DOPO has drawn particular interest. Its structure, centered around a reactive P–H bond, grants it remarkable design versatility—allowing it to react with carbonyl groups, epoxy rings, and even carbon–carbon double bonds [9–11]. Despite these advantages, incorporating DOPO directly into PUA is far from straightforward. When used at low loadings, its flame-retardant effect is underwhelming; when the amount is increased, the plasticizing effect becomes unavoidable, causing a noticeable drop in mechanical strength and a reduction in the glass transition temperature (Tg) of the polymer [12,13]. This creates a fundamental dilemma: how to significantly improve the flame resistance of PUA without sacrificing the mechanical properties that make the material attractive in the first place.

In recent years, considerable effort has been devoted to improving the thermal stability and mechanical performance of polymer composites through the incorporation of inorganic nanofillers [14–17]. Among the numerous candidates, MOFs have emerged as particularly promising for flame-retardant design. Their exceptionally high surface area, adjustable pore architecture, and inherent thermal robustness make them well-suited for constructing multifunctional flame-retardant systems [18–21]. Wei et al. [22] synthesized a cobalt-based metal-organic framework (Co-MOF) featuring a multilayer mesoporous structure formed by the coordination of a phosphorus- and nitrogen-rich organic ligand with cobalt ions. The resulting composite significantly enhanced the flame retardancy, melt-drip resistance, and mechanical properties of polylactic acid. Li et al. [23] successfully balanced the flame retardancy and mechanical properties of the matrix by constructing a hybrid material through *in situ* growth of Co-MOF and chemical grafting of DOPO. In this study, ZIF-67 was selected as the MOF host based on several key considerations. Firstly, ZIF-67 exhibits high thermal stability, which is crucial for maintaining structural integrity during the polymer processing and initial stages of combustion. Secondly, the cobalt (Co) ions within its framework are known for their catalytic activity, particularly in promoting the graphitization of carbonaceous char during thermal degradation, a desirable trait for enhancing condensed-phase flame retardancy. Finally, ZIF-67 itself can yield a relatively high carbon residue upon pyrolysis, providing a physical barrier effect. A growing body of work has shown that integrating organophosphorus compounds with MOFs can trigger a synergistic flame-retardant effect, acting in both the condensed and gas phases during combustion [24–26]. Despite this advantage, many MOF/organophosphorus hybrid flame retardants prepared through simple physical blending suffer from nonuniform dispersion or weak interfacial compatibility within the polymer matrix. These shortcomings often undermine the mechanical integrity of the resulting material, counteracting the intended performance enhancements.

To overcome these challenges, this study introduces a novel design strategy in which DOPO is first grafted onto the surface of ZIF-67, followed by partial amino-functionalization to create an amino-modified DOPO–MOF structure. The incorporated amino groups serve a dual purpose: they enhance the material's flame-retardant performance and, crucially, can chemically react with the –NCO groups in the PUA matrix. This reaction establishes covalent linkages between the flame retardant and polyurea chains, enabling a reactive integration that sidesteps the dispersion problems typically associated with purely physical blending. As a result, the approach not only preserves but can even improve the mechanical properties of PUA. Through this strategy, the study seeks to offer a blueprint for designing PUA composites that achieve both superior flame resistance and robust mechanical stability, providing fresh theoretical insights and practical pathways for the development of reactive flame-retardant systems and their application in high-performance protective materials.

2 Experiments

2.1 Main Raw Materials

Cobalt nitrate hexahydrate ($Co(NO_3)_2·6H_2O$, analytical grade), 2-methylimidazole (99%), N,N-dimethylformamide (DMF, analytical grade), absolute ethanol (analytical grade), methanol (analytical grade), aniline (≥99%), 4-aminoacetophenone (99%), p-toluenesulfonic acid monohydrate (p-TSA, analytical grade), and 9,10-dihydro-9-oxa-10-phosphaphenanthrene-10-oxide (DOPO, 97%) were all purchased from Shanghai Aladdin Biochemical Technology Co., Ltd. All chemicals were of analytical reagent grade and used without further purification. The distilled water used in the experiments was prepared in the laboratory.

2.2 Preparation ZIF-67

ZIF-67 was synthesized according to a previously reported method with appropriate modifications [27–29]. Initially, a measured quantity of cobalt nitrate hexahydrate ($Co(NO_3)_2·6H_2O$, 2.91 g, 10 mmol) was dissolved in 50 mL of methanol under stirring until complete dissolution. Subsequently, 2-methylimidazole (6.49 g, 79 mmol) was dissolved in another 50 mL portion of methanol. The two solutions were then combined and stirred magnetically at room temperature for 24 h, during which the mixture gradually turned purple with observable precipitate formation, indicating the crystallization of ZIF-67. The resulting precipitate was isolated by centrifugation (8000 rpm, 10 min) and washed sequentially with methanol three times to remove unreacted species. Finally, the product was dried under vacuum at 80°C for 12 h, yielding ZIF-67 as a purple powder.

2.3 Preparation ZIF-67@DOPO

A mixture of 10.809 g of DOPO (0.05 mol) and 11.413 g of ZIF-67 (0.05 mol, based on Co content) was first dispersed in 100 mL of DMF within a 250 mL three-neck flask, which was fitted with mechanical stirring and a reflux condenser. The reaction system was then heated and stirred at 80°C–100°C for 6–12 h, allowing the phosphoric groups of DOPO to coordinate effectively with the cobalt ions in ZIF-67, thereby promoting the grafting of DOPO onto the MOF surface. After completion, the mixture was left to cool naturally to room temperature, followed by centrifugation at 5000–8000 rpm to remove the supernatant. The resulting precipitate was subsequently subjected to ultrasonic dispersion in ethanol (or methanol) and washed repeatedly, 3 to 5 times, until the supernatant became colorless and clear. Finally, the purified sample was dried in a vacuum oven at 80°C for 12–24 h, yielding the ZIF-67@DOPO composite.

2.4 Preparation DOPO-NH_2 and ZIF-67@DOPO-NH_2

DOPO-NH_2 was synthesized by reacting DOPO with 4-aminoacetophenone in a molar ratio of 1:1.2 in DMF at 120°C for 8 h under nitrogen atmosphere, using p-toluenesulfonic acid as catalyst. The resulting product was purified by recrystallization from ethanol. It was synthesized specifically to serve as a comparative reference for evaluating the performance of unmodified DOPO when directly incorporated into the polyurea matrix.

An appropriate amount of ZIF-67@DOPO was dispersed in 100 mL of DMF in a 250 mL three-neck flask equipped with mechanical stirring and a reflux condenser. Subsequently, 4-aminoacetophenone (6.758 g, 0.05 mol), aniline (9.314 g, 0.1 mol), and p-toluenesulfonic acid monohydrate (p-TSA, 0.190 g, 0.001 mol) were added as an acidic catalyst. The reaction mixture was stirred at 100°C–130°C for 6–12 h to obtain the amino-functionalized MOF composite. After the reaction, the system was allowed to cool naturally to room temperature. The product was collected by centrifugation and washed repeatedly with ethanol or methanol 3–5 times to remove unreacted monomers and by-products. The resulting solid was

dried in a vacuum oven at 80°C for 24 h, yielding the final amino-functionalized composite material ZIF-67@DOPO-NH_2.

2.5 Preparation of PUA Composites

The PUA composite containing 5 wt% ZIF-67@DOPO-NH_2 was fabricated through the following representative procedure. First, 2.5 g of ZIF-67@DOPO-NH_2 was incorporated into 22.5 g of a curing agent system composed of amino-terminated polyether and an amino-based chain extender. The mixture was transferred to a beaker and subjected to 30 min of vigorous mechanical stirring using a polytetrafluoroethylene impeller, followed by ultrasonic treatment. To eliminate entrapped air bubbles introduced during mixing, the resulting mixture was vacuum-treated in an oven set at 80°C. Subsequently, 25 g of the processed mixture was combined with 25 g of a diphenylmethane diisocyanate (MDI)-based prepolymer, and the blend was poured into a mold to produce the final PUA composite. For comparative purposes, reference samples including pure PUA, PUA/ZIF-67, PUA/ZIF-67@DOPO, PUA/DOPO, and PUA/DOPO-NH_2 were prepared using identical processing parameters to ensure consistency in preparation conditions.

2.6 Characterization

Morphology was examined using a GeminiSEM 500 scanning electron microscope (Carl Zeiss, Germany). Fourier transform infrared (FTIR) spectra were collected using an Avatar 360 spectrophotometer (Nicolet, USA) over the wavenumber range of 400–4000 cm^{-1}. Thermogravimetric analysis (TGA) was performed on a TGA/DSC3+ analyzer (METTLER TOLEDO, Switzerland) under a nitrogen atmosphere, with 5–10 mg samples heated from room temperature to 800°C at a rate of 10°C/min. X-ray diffraction (XRD) measurements were carried out on a Shimadzu XRD-7000 (Shimadzu Corporation, Japan) to analyze the crystal structure, with scans ranging from 12° to 80° (2θ) at 8°/min. X-ray photoelectron spectroscopy (XPS, PHI5000 VersaProbe, ULVAC-PHI Ltd., Japan) under vacuum was used to determine the elemental composition and chemical states of the synthesized flame retardants.

The LOI values were measured with a JF-3 oxygen index meter on samples of dimensions 100 mm^3 × 6.5 mm^3 × 3 mm^3. Vertical UL-94 tests were conducted on a CZF-5 instrument (Nanjing Jiangning Analytical Instrument Co., China) following the IEC 60695-11-10 standard, using samples sized 130 mm^3 × 13 mm^3 × 3 mm^3. Cone calorimeter tests (CCT) were conducted on an FTT (Fire Testing Technology Ltd., UK) apparatus according to ISO 5660, using 100 × 100 × 3 mm^3 samples exposed to a heat flux of 35 kW/m^2. Raman spectra of the residual char were recorded using an Invia Raman microscope (Renishaw, UK) with a 532 nm excitation wavelength.

Tensile properties of the composites were evaluated on a GOTECH TCS-2000 universal testing machine (China) at a constant strain rate of 2.0 mm/min. All tensile tests were conducted at least five times to ensure reproducibility. Dynamic thermomechanical properties of the 33 mm^3 × 10 mm^3 × 10 mm^3 samples were analyzed using a TA Instruments DHR-2 rotational rheometer (USA), with heating from 25°C to 200°C at a rate of 3°C/min.

3 Results and Discussion

3.1 Structural Analyses

To verify the successful construction of the amino-functionalized DOPO-modified metal-organic framework (ZIF-67@DOPO-NH_2) and its reactive incorporation into the polyurea system, this study systematically characterized the material's structure and morphology using SEM, energy-dispersive X-ray spectroscopy (EDS), XRD, FTIR, and XPS.

As shown in Fig. 1a, SEM observations and EDS analysis revealed that the pristine ZIF-67 particles exhibited a well-defined rhombic dodecahedral morphology, which is characteristic of high-purity ZIF-67 crystals [30]. In sharp contrast, the pure DOPO sample appeared as irregular micrometer-sized aggregates (Fig. 1b), highlighting the distinct morphological differences between the two primary components. Notably, after the formation of the ZIF-67@DOPO composite (Fig. 1c), the particles largely preserved the structural framework of the original ZIF-67 precursor, their surfaces became noticeably rougher, with edges appearing somewhat blurred. This pronounced change in surface morphology provides strong evidence for the successful and uniform deposition of DOPO onto the MOF, effectively creating a core–shell structure. Following subsequent amino-functionalization, the final ZIF-67@DOPO-NH_2 product (Fig. 1d) retained a well-dispersed polyhedral shape without signs of structural collapse, suggesting that the post-modification procedure was both gentle and efficient.

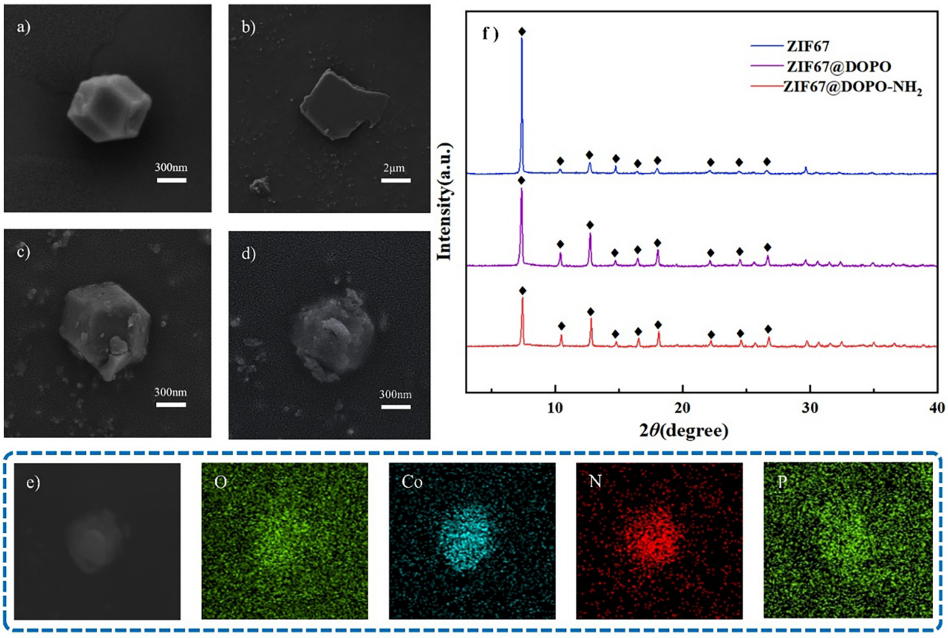

Figure 1: (**a**) SEM images of ZIF-67, (**b**) DOPO, (**c**) ZIF-67@DOPO, and (**d**) ZIF-67@DOPO-NH_2; (**e**) EDS elemental mapping of ZIF-67@DOPO-NH_2; (**f**) XRD spectra of ZIF-67, ZIF-67@DOPO, and ZIF-67@DOPO-NH_2.

Further evidence for the homogeneous composition of the composite was provided by EDS elemental mapping. As shown in Fig. 1e, spatially resolved EDS mapping of ZIF-67@DOPO-NH_2 revealed highly overlapping distributions of key elements: cobalt from the ZIF-67 framework, phosphorus from DOPO, nitrogen from both the imidazolate linker and the introduced amino groups, and oxygen. The uniform and coincident signals of Co and P throughout the entire particle architecture provide direct and compelling evidence for the formation of a homogeneous composite rather than a simple physical mixture. This homogeneous elemental distribution, coupled with the preserved morphology, confirms the successful synthesis of a structurally well-defined ZIF-67@DOPO-NH_2 core-shell composite, a structural characteristic anticipated to be advantageous for its subsequent application performance.

Fig. 1f displays the XRD patterns of ZIF-67, ZIF-67@DOPO, and ZIF-67@DOPO-NH_2. As observed, all three samples exhibit distinct diffraction peaks at 2θ = 7.4°, 10.4°, 12.7°, 14.8°, 16.4°, 18.1°, 24.5°, 26.7°, and 29.6°, which align well with those reported in the literature [27,31]. Compared with pristine ZIF-67, the diffraction peak positions of ZIF-67@DOPO and ZIF-67@DOPO-NH_2 remain largely unchanged, with only

a slight reduction in peak intensity. This indicates that the introduction of DOPO and its amino derivative did not disrupt the crystalline framework of ZIF-67, though it may have influenced the crystal growth process, leading to a decrease in crystallite size or a slight reduction in crystallinity. This observation suggests that DOPO molecules primarily interact with ZIF-67 through surface grafting or pore confinement rather than direct coordination with the Co–Im framework, thereby effectively preserving the ordered structure of the MOF. Furthermore, the more pronounced attenuation of peak intensity in ZIF-67@DOPO-NH_2 may be attributed to stronger coordination or hydrogen bonding interactions involving the amino-DOPO molecules, which could cause more significant perturbation to the crystal surface during the coating process.

To confirm the amino-functionalization of DOPO and its successful composite formation with ZIF-67 at the molecular level, Fourier-transform infrared spectroscopy was performed on all samples, as shown in Fig. 2a. In the FTIR spectrum of DOPO, characteristic absorption peaks of its molecular structure are clearly observed: the sharp peak at 2438 cm^{-1} is attributed to the P–H stretching vibration, which is the most distinctive feature of DOPO; the strong and broad absorption band around 1232 cm^{-1} corresponds to the P=O stretching vibration; while a series of absorption peaks near 907 and 754 cm^{-1} originate from vibrational modes of the P-O-Ph group [32,33]. The spectrum of DOPO-NH_2 exhibits decisive changes. The most notable evidence is the complete disappearance of the characteristic P–H absorption peak at 2438 cm^{-1}, indicating the successful reaction of the P–H bond. Simultaneously, a pair of new absorption peaks emerge at approximately 3370 and 3290 cm^{-1}, corresponding to the asymmetric and symmetric stretching vibrations of the newly introduced –NH_2 groups, respectively. Additionally, the absorption peak near 1601 cm^{-1} can be assigned to the N–H bending vibration, while a shoulder peak around 1150 cm^{-1} likely originates from the C–N stretching vibration. The appearance of these new peaks, together with the disappearance of the P–H peak, constitutes comprehensive spectroscopic evidence for the successful conversion of DOPO to DOPO-NH_2. In the spectrum of the ZIF-67@DOPO composite, characteristic signals from both the ZIF-67 framework and DOPO are observed. Typical absorptions of the imidazolate ligands in ZIF-67, such as the C=N stretching vibration at 1583 cm^{-1} and the Co–N stretching vibration below 500 cm^{-1}, are clearly visible. More importantly, the characteristic P=O absorption peak of DOPO (around 1232 cm^{-1}) remains present, but its position shows a noticeable blue/red shift compared to pure DOPO. This shift is commonly attributed to Lewis acid-base coordination interactions between the P=O groups of DOPO molecules and the metal Co nodes in the ZIF-67 framework, which not only serves as direct evidence of their successful composite formation but also reveals the nature of their interfacial bonding. Finally, the spectrum of ZIF-67@DOPO-NH_2 demonstrates a perfect integration of all expected characteristic peaks, it retains the framework vibration peaks of ZIF-67 (C=N and Co–N), displays the shifted P=O characteristic peak of DOPO-NH_2 due to coordination, and clearly shows the N–H stretching and bending vibrations introduced by amino-functionalization. This spectrum unambiguously confirms the successful preparation of a structurally intact ZIF-67@DOPO-NH_2 composite material, in which the ZIF-67 framework is preserved, DOPO-NH_2 is successfully grafted via coordination, and surface amino functional groups are effectively introduced.

To confirm the successful grafting of ZIF-67 onto DOPO and the subsequent amino-functionalization at the molecular level, a systematic X-ray photoelectron spectroscopy (XPS) analysis was conducted on the final product ZIF-67@DOPO-NH_2. The C 1s spectrum clearly reflects the coexistence of organic components in the composite material. The characteristic peak at 284.8 eV is attributed to C–C/C–H bonds in the benzene rings and alkyl chains of DOPO. The peak at 285.8 eV, which is of critical importance [23,26], represents a combined signal from the C–N bonds in the imidazolate ligands of ZIF-67 and the C–O–P structure in the DOPO derivative. The unambiguous presence of this peak provides direct spectroscopic evidence for the successful progression of the first-step grafting reaction between ZIF-67 and DOPO. The N 1s spectrum

exhibits a distinct doublet at 397.2 and 397.8 eV, whose binding energies are markedly lower than those commonly associated with pyridinic nitrogen or primary amine nitrogen. Such an unusual shift is likely rooted in the strong electron-donating behavior of the DOPO unit, whose influence is transmitted through the molecular backbone. Additionally, possible intramolecular interactions between the amino group and the phosphine oxide (P=O) moiety may further enrich the electron density around the nitrogen atoms, thereby lowering their binding energies. Despite this anomaly, the two well-resolved peaks can still be assigned to the imidazole nitrogen within the ZIF-67 framework and the nitrogen-containing functionalities introduced during the amination step, confirming the successful execution of the second-step modification.

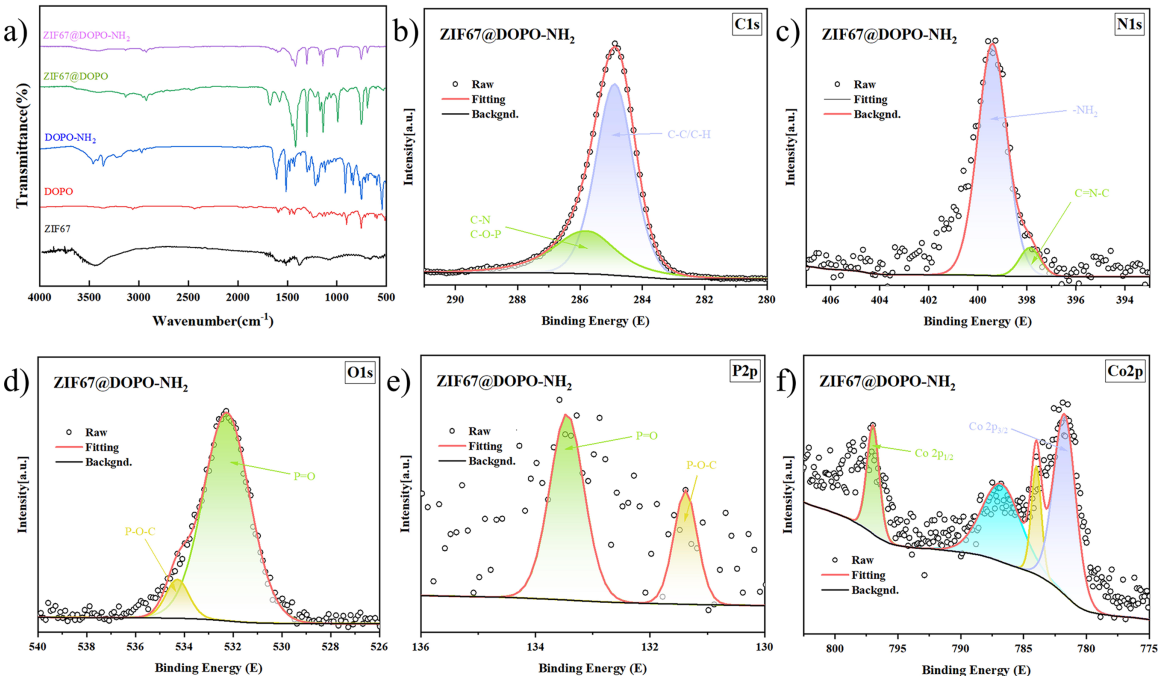

Figure 2: (**a**) FTIR spectra of ZIF-67, DOPO, DOPO-NH_2, ZIF-67@DOPO, and ZIF-67@DOPO-NH_2; XPS spectra of ZIF-67@DOPO-NH_2; C 1s (**b**), N 1s (**c**), O 1s (**d**), P 2p (**e**), Co 2p (**f**).

A deeper examination of the interfacial chemical environment highlights the origin of the composite's robust bonding characteristics. In the O 1s spectrum, the dominant peak centered at 532.2 eV corresponds to the P=O group of the DOPO structure. Similarly, the characteristic peak at 133.3 eV in the P $2p_3/_2$ region represents the phosphorus atom in the O=P–O–Ph environment. The binding energy features of these two elements are in excellent agreement with those observed in the Co 2p spectrum. Specifically, the Co $2p_3/_2$ main peak at 781.0 eV, accompanied by a pronounced shoulder at 783.5 eV, indicates that Co(II) ions exist in multiple coordination states. This spectral signature strongly supports the formation of coordination interactions between the DOPO P=O groups and the Co(II) nodes in ZIF-67—namely, the P=O→Co coordination bond. This bond represents the central mechanism driving the first-step grafting reaction and ensures the structural integrity of the hybrid system, thereby enabling robust synergy among the flame-retardant components. In summary, the XPS results validate the successful construction of the ZIF-67@DOPO-NH_2 composite as intended. Beyond confirming the coexistence of the ZIF-67 framework, DOPO units, and amino functionalities, the spectral evidence unequivocally demonstrates the formation of P=O→Co coordination bonds, shedding light on the precise chemical bonding architecture that underpins the composite's stability and flame-retardant performance.

3.2 Flame Retardant Properties

The vertical burning test results (Fig. 3 and Table 1) clearly reveal how different flame-retardant systems influence the combustion behavior of PUA. The pure PUA sample (a) exhibited intense dripping during combustion and continued to burn after both ignitions; the molten droplets ignited the underlying cotton, which sustained flaming for 123 s, highlighting the material's inherently high flammability. When DOPO was introduced (b), the sample displayed partial self-extinguishing behavior; however, dripping remained significant, resulting in cotton ignition lasting 86 s. Further modification to DOPO-NH_2 (c) enhanced flame retardancy, no dripping occurred during the first ignition, although dripping and subsequent cotton ignition reappeared during the second ignition test. It is worth noting that the DOPO-NH_2 sample serves as a critical control, which helps to decouple the contribution of the amino functionalization itself (e.g., improved compatibility and potential gas-phase dilution) from the effects arising from the MOF core-shell structure and its catalytic activity. A notable shift occurred with the incorporation of ZIF-67 (d). Dripping during combustion was substantially reduced, and the cotton burning time decreased to 46 s, demonstrating the MOF's effective condensed-phase role in stabilizing the molten polymer and inhibiting liquid-phase dripping. The ZIF-67@DOPO composite system (e) exhibited excellent self-extinguishing capability, rapidly extinguishing after both ignitions; however, flaming droplets still ignited the cotton, indicating that dripping suppression had not yet been fully resolved. In contrast, the ZIF-67@DOPO-NH_2 composite (f) delivered the most comprehensive improvement. The sample self-extinguished rapidly after both ignitions and, crucially, eliminated cotton ignition entirely by preventing the generation of flaming droplets. This superior performance underscores the validity of the design strategy: ZIF-67 and DOPO synergistically provide rapid gas- and condensed-phase flame inhibition, while amino functionalization enhances interfacial compatibility and reactive integration with the polyurea matrix, effectively suppressing combustion-induced dripping and markedly elevating overall fire safety.

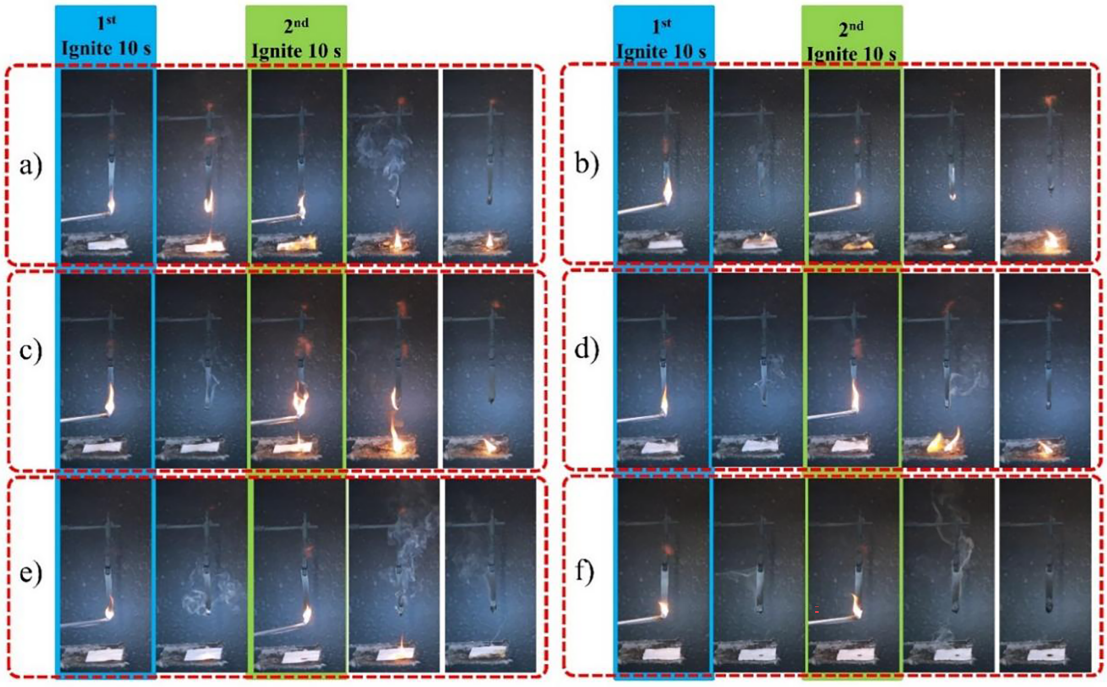

Figure 3: Digital photos of PUA (**a**), PUA/DOPO (**b**), PUA/DOPO-NH_2 (**c**), PUA/ZIF-67 (**d**), PUA/ZIF-67@DOPO (**e**), and PUA/ZIF-67@DOPO-NH_2 (**f**) samples in UL-94 testing.

Table 1: UL-94 and LOI test results for PUA and PUA composites.

Sample	LOI (%)	Ul-94				
		t_1 (s)	t_2 (s)	t_3 (s)	Ignition of Cotton	Rating
PUA	19.2	17	13	123	YES	V-2
PUA/DOPO	20.5	0	16	86	YES	V-2
PUA/DOPO-NH_2	21.8	0	7	92	YES	V-2
PUA/ZIF-67	21.0	0	3	46	YES	V-2
PUA/ZIF-67@DOPO	22.6	0	0	23	YES	V-2
PUA/ZIF-67@DOPO-NH_2	23.8	0	0	0	NO	V-0

The pure polyurea sample exhibited a low LOI value of 19.2% and showed intense burning accompanied by severe dripping in the UL-94 test, demonstrating its intrinsically high flammability. The addition of physically blended DOPO slightly increased the LOI to 20.5%; however, pronounced dripping still occurred, underscoring the limited effectiveness of a solely gas-phase flame-retardant mechanism. When DOPO was amino-functionalized (DOPO-NH_2), the LOI further increased to 21.8%, which can be attributed to its improved compatibility with the polyurea matrix resulting from higher molecular polarity. The performance of DOPO-NH_2 alone establishes a baseline for the "amino-functionalization effect," against which the superior performance of the ZIF-67-integrated hybrid can be compared. Nevertheless, dripping during UL-94 testing remained unresolved. Incorporating unmodified ZIF-67 yielded an LOI of 21.0%. Although the porous framework of ZIF-67 provided a certain physical barrier effect in the condensed phase, its individual chemical inhibition capability was still insufficient to deliver satisfactory flame retardancy. In contrast, the ZIF-67@DOPO composite system produced a substantial improvement, raising the LOI to 22.6% and achieving self-extinguishing behavior in the UL-94 test for the first time. This enhancement results from the synergistic interaction between the radical-quenching action of DOPO in the gas phase and the catalytic char-forming effect of ZIF-67 in the condensed phase. The reactively grafted ZIF-67@DOPO-NH_2 composite exhibited the best overall performance, reaching an LOI of 23.8% and achieving a UL-94 V-0 rating with completely drip-free combustion. This exceptional flame-retardant behavior derives from a multi-stage synergistic mechanism: the DOPO moiety releases ·PO· radicals to terminate gas-phase combustion chain reactions; the thermally transformed cobalt oxide species (e.g., Co_2O_3) from ZIF-67 catalyze the formation of a dense and coherent char layer; and the amino groups further enhance interfacial compatibility, promoting the development of a more stable and continuous protective char structure.

Cone calorimeter testing, recognized as one of the most reliable methods for simulating real fire scenarios, provides a set of key parameters that collectively describe the combustion behavior of polymer materials. Fig. 4 illustrates the heat release rate (HRR), total heat release (THR), smoke production rate (SPR), and total smoke production (TSP) curves for pure PUA and the flame-retardant-modified PUA composites, with the corresponding characteristic data summarized in Table 2. As shown, the unmodified PUA exhibits extremely high fire sensitivity. Its Time to Ignition (TTI) is only 8 s, a reflection of its inherently unstable chemical structure that allows it to decompose rapidly and reach combustion conditions under even short heat exposure. The introduction of flame-retardant systems significantly improved the ignition resistance of the composites. When DOPO or DOPO-NH_2 was incorporated through physical blending, the TTI values were extended to 22–23 s, indicating a noticeable delay in the onset of combustion. The addition of ZIF-67 produced a distinct influence, further modifying the ignition behavior of the matrix. Among all samples, the PUA/ZIF-67@DOPO-NH_2 composite exhibited the most pronounced improvement,

achieving a TTI of 25 s, an extension of 212% compared with pure PUA. This substantial enhancement arises from the cooperative action of amino-functionalized DOPO and ZIF-67. ZIF-67 contributes by increasing the thermal stability of the polymer matrix and slowing its initial decomposition. Meanwhile, during the early heating stage, DOPO-NH_2 releases phosphorus-containing free radicals capable of quenching the combustion chain reaction. Together, these effects effectively delay ignition and provide superior protection against heat-induced thermal degradation.

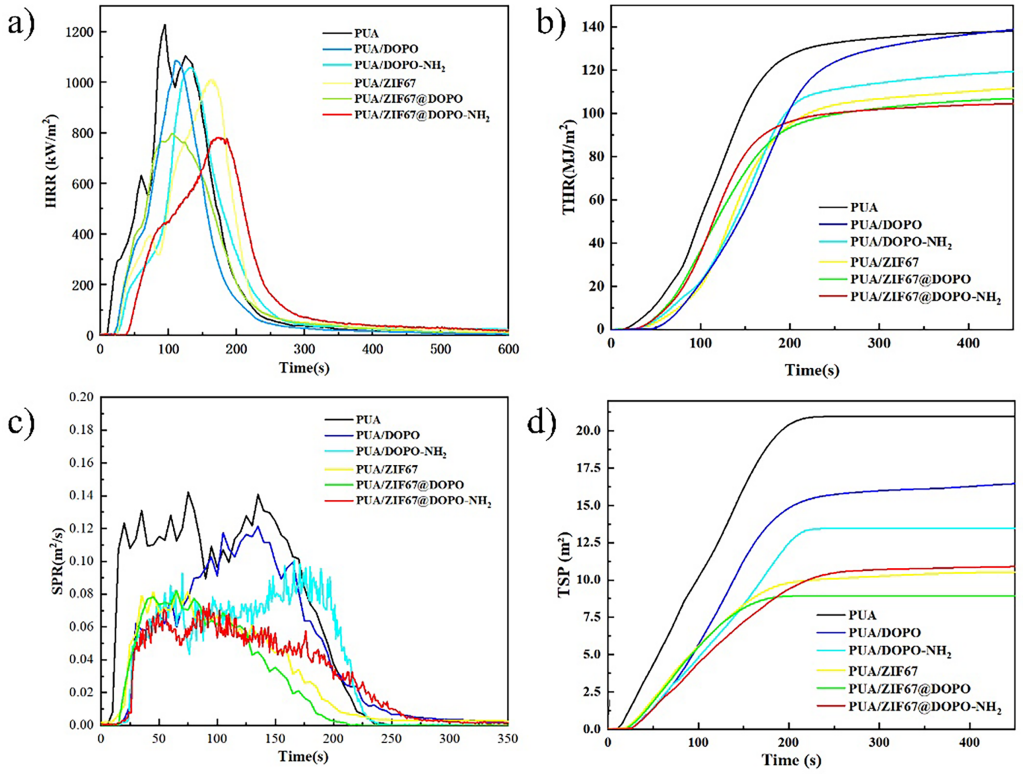

Figure 4: HRR (**a**), THR (**b**), SPR (**c**), TSP (**d**) curves.

Table 2: FPI and FGI values of PUA composites.

Sample	TTI	pHRR	TTP	TSP	FPI	FGI	SF
	(s)	(kW/m^2)	(s)	(m^2)	(m^2·s/kW)	(kW/m^2·s)	(MW/m^2)
PUA	8	1227.03	95	20.97	0.0065	12.92	25.73
PUA/DOPO	23	1085.30	110	16.61	0.0212	9.87	18.03
PUA/DOPO-NH_2	22	1069.05	132	13.49	0.0206	8.10	14.42
PUA/ZIF-67	19	1009.23	166	10.92	0.0188	6.08	11.02
PUA/ZIF-67@DOPO	18	797.61	105	10.54	0.0226	7.60	8.41
PUA/ZIF-67@DOPO-NH_2	25	781.51	174	8.95	0.0320	4.49	6.99

The analysis of heat release behaviors provides deeper insight into how the flame-retardant system suppresses fire intensity. Pure PUA exhibits a sharp, almost violent combustion pattern, with its Peak Heat Release Rate (pHRR) reaching an exceptionally high 1227.03 kW/m^2, a clear indication of rapid and

uncontrolled heat release. Once single-component flame retardants were incorporated, this value began to decline, albeit to different extents. For instance, PUA/DOPO and PUA/DOPO-NH_2 displayed moderately reduced pHRR values of 1085.30 and 1069.05 kW/m^2, corresponding to decreases of roughly 11%–13%. The introduction of ZIF-67 alone provided an even more noticeable improvement, bringing the pHRR down to 1009.23 kW/m^2. The most remarkable transformation emerged only when both organic (DOPO-based) and inorganic (ZIF-67-derived) flame-retardant components were integrated into a unified system. The composite PUA/ZIF-67@DOPO sample exhibited a dramatic drop in pHRR to 797.61 kW/m^2, and PUA/ZIF-67@DOPO-NH_2 further pushed this value down to just 781.51 kW/m^2. In comparison to pristine PUA, this represents an impressive 36.3% reduction, an unmistakable signal of a synergistic, rather than merely additive, flame-retardant effect. This powerful suppression of pHRR originates from a dual-phase flame-retardant mechanism. In the condensed phase, ZIF-67 and its thermolysis products catalyze the formation of a compact, continuous, and highly graphitized char layer. Such a barrier sharply limits heat feedback and hinders the outward diffusion of volatile fuel fragments. Simultaneously, in the gas phase, DOPO-derived PO· and HPO· radicals disrupt the combustion chain reaction by scavenging high-energy radicals such as H· and OH·. The interplay of these two mechanisms, one physically isolating, the other chemically quenching, produces a highly efficient suppression of the combustion process. The evolution of Total Heat Release (THR) offers further confirmation of this synergy. While pure PUA exhibits a THR of 25.73 MJ/m^2, all flame-retardant-modified formulations show significant reductions. Notably, PUA/ZIF-67@DOPO-NH_2 achieves a THR as low as 6.99 MJ/m^2, reflecting a 72.8% decrease. Such a substantial reduction demonstrates that the composite system not only weakens the peak fire intensity but also delays and diminishes the overall energy released throughout combustion, a crucial criterion for achieving meaningful fire-safety enhancement in polymer materials.

Smoke production characteristics constitute another critical dimension in assessing the overall fire safety of polymeric materials. During combustion, pristine PUA released a considerable amount of smoke, with its Total Smoke Production (TSP) soaring to 20.97 m^2. Once flame retardants were incorporated, however, this parameter exhibited a remarkable decline. In particular, the ZIF-67–derived composites displayed pronounced smoke-suppression capabilities. Among them, PUA/ZIF-67@DOPO-NH_2 delivered the most striking improvement, with its TSP value reduced to merely 8.95 m^2, corresponding to a 57.3% decrease relative to the unmodified matrix. This substantial mitigation of smoke generation can be traced primarily to the catalytic char-forming behavior imparted by ZIF-67. The presence of cobalt-based nodes and the phosphorus–nitrogen functionalities accelerates the construction of a compact, thermally stable char layer during combustion. Such a barrier not only impedes the escape of volatile pyrolysis fragments but also intercepts soot precursors, effectively suppressing the formation and release of smoke at its origin. As a result, the composite exhibits a far safer combustion profile, combining reduced smoke emissions with enhanced structural protection under fire conditions.

Fire risk assessment was conducted through comprehensive parameters including the Fire Performance Index (FPI) and Fire Growth Index (FGI). FPI, defined as the ratio of TTI to pHRR, reflects the material's fire safety margin. The FPI value of pure PUA was only 0.0065 m^2·s/kW, while after flame retardant modification it increased significantly, with PUA/ZIF-67@DOPO-NH_2 achieving an FPI of 0.0320 m^2·s/kW, an increase of nearly 5 times, indicating a qualitative leap in fire safety. FGI, characterized by the ratio of pHRR to Time to Peak (TTP), represents the fire development rate. The FGI value of pure PUA was 12.92 kW/m^2·s, while that of PUA/ZIF-67@DOPO-NH_2 decreased to 4.49 kW/m^2·s, a reduction of 65.2%, proving that the fire development rate is effectively controlled. Furthermore, the Smoke Factor (SF), as a comprehensive indicator for assessing smoke hazard, is calculated as the product of pHRR and TSP. The SF value of pure PUA was as high as 25.73 MW/m^2, while that of PUA/ZIF-67@DOPO-NH_2 decreased to 6.99 MW/m^2, a reduction of

72.8%. This result further confirms the composite material's outstanding performance in reducing the harm caused by smoke.

3.3 Flame Retardant Mechanism

Fig. 5 presents the morphology of the residual char and the corresponding Raman spectroscopy analysis for the series of polyurea composites after cone calorimeter testing. The SEM images of the char residues (Fig. 5a–f) clearly illustrate the pronounced influence of different flame-retardant systems on the development and integrity of the condensed-phase char. The pure PUA sample (Fig. 5a) produced almost no coherent char layer after combustion; only scattered, fragile carbon fragments were observed, with the underlying fumed-silica cubic framework extensively exposed. This morphology reflects the inherently poor condensed-phase flame-retardant capability of the pristine polymer. Upon incorporation of DOPO (Fig. 5b) or DOPO-NH_2 (Fig. 5c), the char coverage improved to a certain degree. Nevertheless, portions of the silica skeleton remained visible, and the resulting char layers were still porous and loosely connected, suggesting that the condensed-phase protection afforded by these physically incorporated additives remained insufficient.

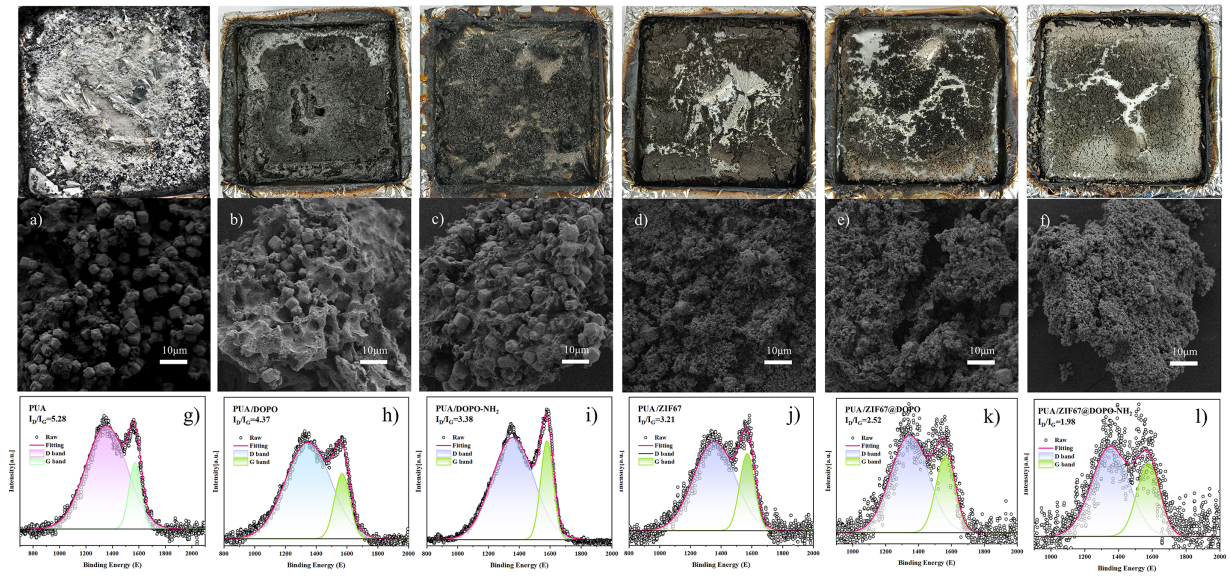

Figure 5: (**a**–**f**) Digital photographs and SEM images of residual carbon of PUA composites; (**g**–**l**) Raman spectra of residual carbon of PUA composites.

When ZIF-67 was incorporated into the system (Fig. 5d), the char morphology improved markedly. The resulting residue exhibited partial encapsulation of the silica skeleton, demonstrating that ZIF-67 can effectively catalyze matrix cross-linking and promote char formation at elevated temperatures. Upon further constructing the ZIF-67@DOPO composite (Fig. 5e), the char layer became more compact and continuous, fully covering the silica framework. This improvement clearly reflects the synergistic condensed-phase char-forming capability between ZIF-67 and DOPO. The optimal formulation, PUA/ZIF-67@DOPO-NH_2 (Fig. 5f), yielded a fully developed, dense, and expanded char layer that nearly enveloped the entire filler skeleton. Such an intact barrier significantly enhances thermal insulation while simultaneously inhibiting mass transfer of combustible volatiles.

Raman spectroscopy (Fig. 5g–l) provides further microstructural evidence supporting these observations. The ID/IG values were determined from the ratio of the peak heights of the D band

(~1350 cm^{-1}) and G band (~1580 cm^{-1}) in the baseline-corrected Raman spectra, serving as an indicator of the char's graphitization degree. The ID/IG ratios decrease progressively across the sample series—5.28 (PUA), 4.37 (PUA/DOPO), 3.38 (PUA/DOPO-NH_2), 3.21 (PUA/ZIF-67), 2.52 (PUA/ZIF-67@DOPO), and finally 1.98 (PUA/ZIF-67@DOPO-NH_2). This monotonic decline signifies a continual enhancement in char graphitization, indicating fewer structural defects and a higher degree of ordering. The exceptionally low ID/IG value for PUA/ZIF-67@DOPO-NH_2 confirms the formation of more graphitic microcrystals within the residue, which endows the char with superior thermal stability and barrier performance.

In summary, the ZIF-67@DOPO-NH_2 flame-retardant system developed in this study achieves a highly efficient dual-phase synergy in polyurea. In the gas phase, DOPO-NH_2 functions as an active radical scavenger, suppressing flame propagation by interrupting combustion chain reactions. In parallel, ZIF-67 catalyzes the formation of a dense, continuous, and highly graphitized char layer in the condensed phase, which effectively impedes heat transfer and restricts the diffusion of flammable decomposition products. This coordinated multi-phase mechanism substantially elevates the overall fire safety of the material.

Based on comprehensive characterization, the flame-retardant mechanism of the ZIF-67@DOPO-NH_2 system arises from a sophisticated synergistic interplay between the condensed and gas phases. In the condensed phase, ZIF-67 assumes a central role. During thermal decomposition, ZIF-67 derivatives, presumably cobalt-based oxides, function as highly efficient catalysts, markedly promoting the graphitization of carbon sources derived from the degradation of both the polyurea matrix and the DOPO-NH_2 component. This catalytic effect facilitates the formation of a continuous, dense, and highly graphitized char layer, as evidenced by the lowest ID/IG ratio (1.98) observed in Raman spectroscopy and corroborated by SEM images revealing complete coverage of the silica skeleton. Such a robust char layer acts as an exceptional physical barrier, insulating the underlying polymer from heat and impeding the release of volatile decomposition products, thereby substantially reducing both the HRR and THR.

Simultaneously, in the gas phase, DOPO-NH_2 plays a critical role in flame inhibition. Upon exposure to heat, DOPO-NH_2 undergoes thermal decomposition, generating active species such as PO· and HPO· radicals. These radicals efficiently scavenge the highly reactive H· and OH· radicals present in the flame zone, which are essential for propagating the combustion chain reaction. This radical quenching mechanism in the gas phase not only suppresses flame propagation but also contributes to a notable increase in the LOI. Furthermore, the amino functionality of DOPO-NH_2 facilitates covalent bonding with the polyurea matrix, ensuring homogeneous dispersion, and may additionally promote the generation of non-combustible gases such as NH_3, which help dilute flammable volatiles.

In conclusion, the ZIF-67@DOPO-NH_2 composite achieves outstanding flame-retardant performance in polyurea through a well-coordinated dual-phase mechanism. In the condensed phase, ZIF-67 catalyzes the formation of a dense, graphitized char layer that enhances the physical barrier effect, while in the gas phase, DOPO-NH_2 actively scavenges radicals and dilutes combustible gases. The synergistic interaction between these condensed- and gas-phase processes significantly suppresses both the ignitability and the intensity of combustion, demonstrating a highly effective and cooperative flame-retardant system.

3.4 Thermal Performance

The thermal stability and decomposition behavior of the flame retardants and their corresponding polyurea composites were systematically investigated under a nitrogen atmosphere, as illustrated in Fig. 6. Thermogravimetric analysis of the pristine flame-retardant additives (Fig. 6a,b) reveals distinct and characteristic thermal behaviors. The residual char yield at 900°C shows a clear hierarchy in thermal stability: ZIF-67 exhibits the highest residue mass, followed by ZIF-67@DOPO and ZIF-67@DOPO-NH_2, whereas DOPO and its amino-functionalized derivative generate significantly lower char. This trend underscores the

superior thermal robustness imparted by the ZIF-67 framework and highlights its pivotal role in promoting char formation when combined with phosphorus-containing compounds.

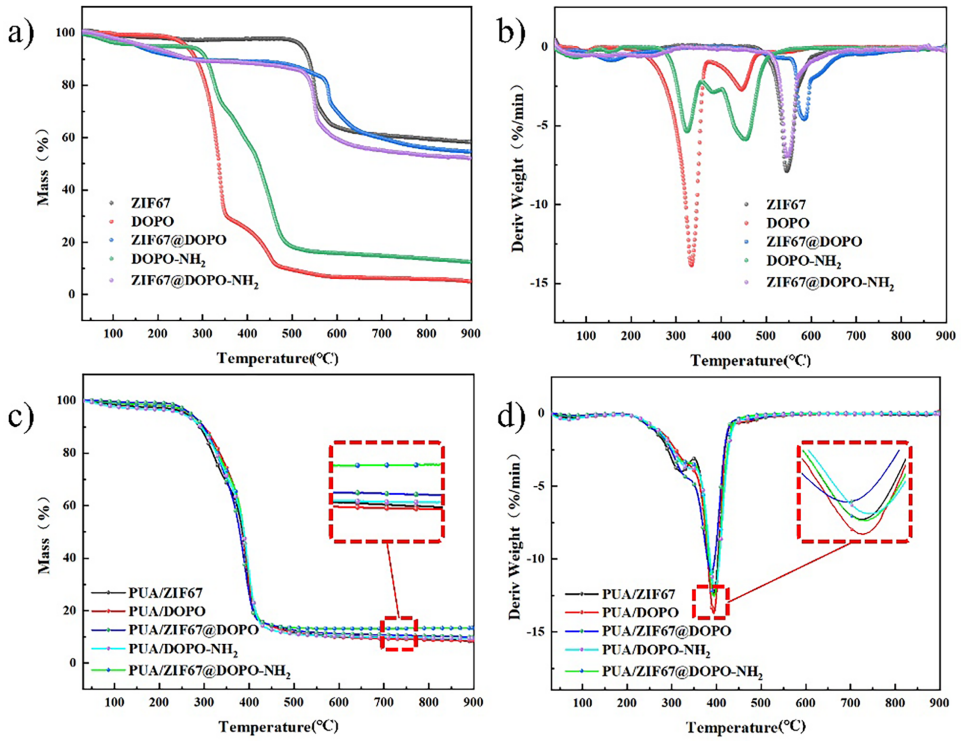

Figure 6: (**a**) TGA curves and (**b**) DTG curves of ZIF-67, DOPO, ZIF-67@DOPO, DOPO-NH_2, and ZIF-67@DOPO-NH_2; (**c**) TGA and (**d**) DTG curves of pure PUA and PUA composites.

Derivative thermogravimetry (DTG) curves provide further insight into the decomposition kinetics. DOPO undergoes a sharp mass loss at 334°C, corresponding to rapid volatilization. In contrast, DOPO-NH_2 exhibits a two-stage decomposition process, with peaks at 324°C and 455°C, reflecting the altered thermal behavior induced by amino-functionalization. Notably, the ZIF-67-containing hybrid systems demonstrate markedly enhanced thermal resilience, with their maximum decomposition rates shifting to significantly higher temperatures in the range of 545°C–584°C. These results confirm the stabilizing effect of the ZIF-67 coordination framework, which not only delays decomposition but also facilitates the formation of thermally robust char structures.

The thermal degradation behavior of the PUA composites (Fig. 6c,d) closely correlates with their flame-retardant performance. The char yield at 900°C exhibits a systematic increase across the series, with PUA/ZIF-67@DOPO-NH_2 showing the highest residual mass, followed sequentially by PUA/ZIF-67@DOPO, PUA/DOPO-NH_2, PUA/ZIF-67, and PUA/DOPO. This ascending trend mirrors the flame-retardant efficacy observed in combustion tests. While all composites undergo their main decomposition stage near 400°C, corresponding to the degradation of the polyurea matrix, the DTG peak intensities vary significantly. Notably, the PUA/ZIF-67@DOPO-NH_2 composite displays a broadened and diminished mass loss rate peak, suggesting a modified thermal decomposition pathway. This behavior arises from the formation of a robust, protective char layer that effectively impedes heat transfer and volatile release during combustion, thereby enhancing flame-retardant performance.

3.5 Mechanical Properties

The mechanical test results (Fig. 7) indicate that the method of flame-retardant incorporation exerts a substantial influence on the tensile properties of polyurea materials. Pristine PUA displayed a tensile strength of 25.74 MPa with an elongation at break of 398%. Interestingly, when DOPO was introduced via physical blending, the resulting PUA/DOPO composite exhibited a notable decrease in tensile strength to 15.53 MPa, accompanied by a decrease in elongation at break to 384%. This change in strength and toughness is likely due to the plasticizing effect of DOPO molecules within the polymer matrix. Remarkably, amino functionalization significantly mitigated this decline, the tensile strength of the PUA/DOPO-NH_2 composite material reached 24.75 MPa, representing a significant improvement over PUA/DOPO while maintaining an elongation at break of 321%. This result underscores the intrinsic benefit of amino functionalization in enhancing interfacial adhesion within a simple blended system. By comparing this with the ZIF-67@DOPO-NH_2 composite, the additional mechanical reinforcement provided by the reactive integration with the robust MOF framework becomes evident. These observations confirm that the amino groups effectively alleviate DOPO's plasticizing influence by improving interfacial compatibility between the flame retardant and the polyurea matrix.

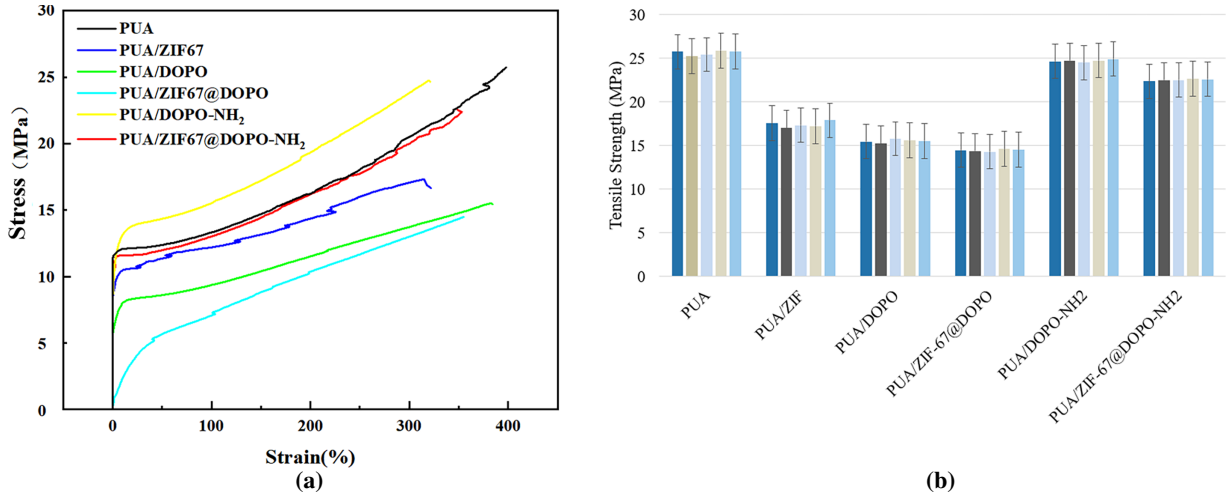

Figure 7: Stress-strain curve diagram (**a**) and parallel sample error diagram of PUA composites (**b**).

Within the ZIF-67 series of composites, PUA/ZIF-67 exhibited a tensile strength of 17.33 MPa and an elongation at break of 322%. The observed reduction in strength is likely due to interfacial defects between the ZIF-67 particles and the polymer matrix. Introducing the ZIF-67@DOPO composite system increased the elongation at break to 355%, tensile strength further declined to 14.48 MPa, highlighting that simple physical compounding remains insufficient to address interfacial discontinuities. The PUA/ZIF-67@DOPO-NH_2 composite exhibited high performance, with tensile strength decreasing by only 12.5% compared to pure PUA, reaching 22.52 MPa, while elongation at break decreased by 11.3%. This outstanding mechanical performance arises from covalent bonding between amino functional groups and isocyanate groups in the polyurea matrix, enabling molecular-level integration of the flame retardant with the polymer network and effectively eliminating interfacial defects. Moreover, the synergistic interplay between the rigid ZIF-67 framework and the flexible DOPO-NH_2 segments optimizes stress transfer throughout the material, enhancing toughness without compromising strength.

SEM micrographs of the tensile fracture surfaces (Fig. 8) provide direct insight into the failure mechanisms. The pure PUA exhibited a rough surface with dense fibrils, indicative of ductile fracture. In contrast,

PUA/DOPO showed a smoother surface with reduced plastic deformation, consistent with its plasticizing effect. The PUA/DOPO-NH_2 surface appeared coarser, suggesting improved compatibility. Notably, PUA/ZIF-67 and PUA/ZIF-67@DOPO composites revealed obvious particle pull-outs and voids, evidencing weak interfacial adhesion and explaining their inferior strength. Remarkably, the PUA/ZIF-67@DOPO-NH_2 composite displayed a uniformly rough, ductile fracture surface without visible particle detachment. This morphology confirms that the reactive integration via covalent bonding effectively eliminated interfacial defects, enabled efficient stress transfer, and was responsible for the optimal balance of retained tensile strength and high elongation at break.

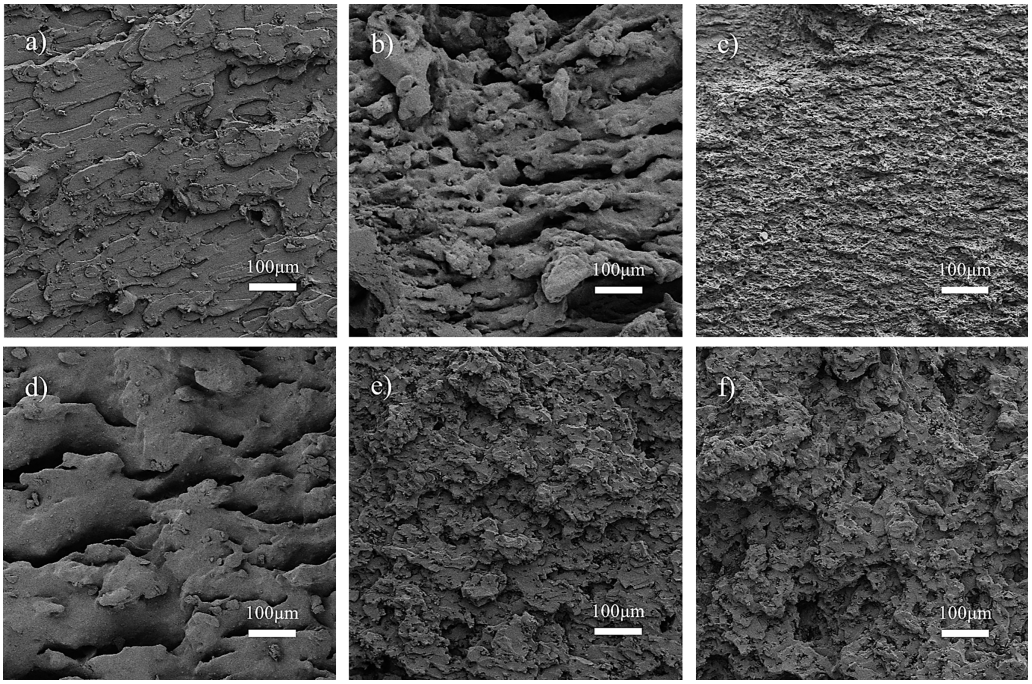

Figure 8: SEM images of PUA (**a**), PUA/ZIF-67 (**b**), PUA/DOPO (**c**), PUA/ZIF-67@DOPO (**d**), PUA/DOPO-NH_2 (**e**), and PUA/ZIF-67@DOPO-NH_2 (**f**).

4 Concluding

This study presents a successful development of an active flame-retardant strategy based on amino-functionalized ZIF-67@DOPO, effectively addressing the long-standing challenge of simultaneously achieving high flame retardancy and mechanical performance in PUA. Comprehensive characterization confirms that DOPO-NH_2 is covalently grafted onto the surface of ZIF-67, with terminal amino groups engaging in chemical reactions with isocyanate groups in the PUA matrix. This transformation shifts the flame-retardant incorporation from conventional "physical mixing" to true "chemical bonding." Such a molecular-level interfacial design not only eliminates defects commonly associated with physical blending but also establishes stable pathways for stress transfer, thereby enhancing the material's mechanical synergy. The flame-retardant system exhibits pronounced synergistic effects across both condensed and gas phases. Under elevated temperatures, ZIF-67 catalyzes the formation of a dense, graphitized carbon layer, serving as an efficient thermal barrier. Simultaneously, DOPO-NH_2 releases active radicals in the gas phase, effectively quenching combustion chain reactions. This dual-phase mechanism enables the composite to achieve a limiting oxygen index of 23.8% and a UL-94 V-0 rating with only 5 wt% additive, while simultaneously reducing the peak heat release rate and total heat release by 36.3% and 38.7%, respectively. The strategy

of reactive integration also enhances mechanical performance. The PUA/ZIF-67@DOPO-NH_2 composite maintains an impressive elongation at break of 353% while reaching a tensile strength of 22.52 MPa, illustrating its unique capacity to overcome the typical trade-off between flame retardancy and mechanical integrity. Overall, this work not only introduces an innovative design paradigm for improving polyurea performance but also provides valuable insights and guidance for interfacial engineering strategies in other polymer-based functional composites.

Acknowledgement: Not applicable.

Funding Statement: This work is financially supported by Natural Science Foundation of Shandong Province (Grant No. ZR2021ME019).

Author Contributions: The authors confirm contribution to the paper as follows: Conceptualization, Mingliang Ma and Yifan Wang; methodology, Yifan Wang; validation, Xishun Qiu, Chao Wu and Jiazhao Li; formal analysis, Chang Dai; investigation, Bowen Han; resources, Mingliang Ma; data curation, Jiazhao Li; writing—original draft preparation, Yifan Wang; writing—review and editing, Mingliang Ma and Ye-Tang Pan; visualization, Jinhu Hu; supervision, Ye-Tang Pan; project administration, Chang Dai; funding acquisition, Mingliang Ma. All authors reviewed and approved the final version of the manuscript.

Availability of Data and Materials: The authors confirm that the data supporting the findings of this study are available within the article.

Ethics Approval: Not applicable.

Conflicts of Interest: The authors declare no conflicts of interest.

References

1. Guo K, Liu J, Qu J, Liu Q, Yu J, Chen R, et al. Dynamic adaptive dual-network synergy achieves high strength and high toughness in polyurea for impact resistance. Chem Eng J. 2025;526(10):171010. doi:10.1016/j.cej.2025.171010.
2. Madelatparvar M, Hosseini MS, Zhang C. Polyurea micro-/nano-capsule applications in construction industry: a review. Nanotechnol Rev. 2023;12(1):20220516. doi:10.1515/ntrev-2022-0516.
3. Shojaei B, Najafi M, Yazdanbakhsh A, Abtahi M, Zhang C. A review on the applications of polyurea in the construction industry. Polym Adv Technol. 2021;32(8):2797–812. doi:10.1002/pat.5277.
4. Guo K, Qu J, Chen R, Liu Q, Yu J, Liu J, et al. A hierarchical energy dissipation strategy for impact-resistant polyurea driven by multiple hydrogen bonds. Constr Build Mater. 2025;487:142056. doi:10.1016/j.conbuildmat.2025.142056.
5. Wang Y, Ding L, Lin J, Qiu X, Wu C, Liu C, et al. Recent developments in polyurea research for enhanced impact penetration resistance and blast mitigation. Polymers. 2024;16(3):440. doi:10.3390/polym16030440.
6. Li Y, Yang H, Chen X, Liu D. Physicochemical mechanism of flame-retardant enhancement for elastomeric polyurea: a mini-review. J Polym Sci. 2025;63(2):358–71. doi:10.1002/pol.20240453.
7. Dukarski W, Rykowska I, Krzyżanowski P, Gonsior M. Flame retardant additives used for polyurea-based elastomers—a review. Fire. 2024;7(2):50. doi:10.3390/fire7020050.
8. Pan YT, Li T, Cao J, Wang DY, Yang R. Advances in reticular materials for flame retardant polymers. Int Mater Rev. 2025;70(7):551–75. doi:10.1177/09506608251345756.
9. Bifulco A, Varganici CD, Rosu L, Mustata F, Rosu D, Gaan S. Recent advances in flame retardant epoxy systems containing non-reactive DOPO based phosphorus additives. Polym Degrad Stab. 2022;200:109962. doi:10.1016/j.polymdegradstab.2022.109962.
10. Qin JY, Zhang WC, Yang RJ. Intercalation process in the preparation of 9,10-dihydro-9-oxa-10-phosphaphenanthrene-10-oxide-montmorillonite nanocompounds and their application in epoxy resins. Mater Des. 2019;178(5):107834. doi:10.1016/j.matdes.2019.107834.

11. Zhang Y, Wang B, Xia Y, Zhang L, Zhu Y, Guo Z, et al. Highly flame retardant and thermal conductive epoxy composites using curing agent and boron nitride modified by phosphorus containing group. J Therm Anal Calorim. 2024;149:14687–98. doi:10.1007/s10973-024-13802-4.
12. Wang J. A novel phosphorus/silicon-containing flame retardant—functionalized graphene nanocomposite: preparation, characterization and flame retardancy. Russ J Appl Chem. 2020;93(12):1931–9. doi:10.1134/s1070427220120162.
13. Jia L, Zhang WC, Tong B, Yang RJ. Crystallization, mechanical and flame-retardant properties of poly(lactic acid) composites with DOPO and DOPO-POSS. Chin J Polym Sci. 2018;36(7):871–9. doi:10.1007/s10118-018-2098-7.
14. Fang J, Dong Y, Lu S, Liu J, Ai L, Liu P. Preparation of polyurea elastomer with flame retardant, insulation and thermal conductivity properties. J Wuhan Univ Technol Mater Sci Ed. 2024;39(3):781–9. doi:10.1007/s11595-024-2937-z.
15. Fan J, Zhang J. Preparation of self-healing thermoplastic polysiloxane-polyurea/polyether-polyurea elastomer blends with a co-continuous microphase structure and in-depth research on their synergistic effects. ACS Appl Mater Interfaces. 2024;16(40):54885–96. doi:10.1021/acsami.4c12019.
16. Qian X, Jiang S. Modification of graphene with organic/inorganic silicon-based materials and its reinforcement on the UV-curing polyurethane composite coatings. Polym Compos. 2018;39(3):746–54. doi:10.1002/pc.23992.
17. Qiu X, Wang Y, Wu C, Li J, Dai C, Han B, et al. "Two-birds-one-stone" strategy: phytic acid-chelated MOFs and $NiMoO_4$ nanorods integrated polyurea for multifunctional flame retardancy, mechanical, and UV protection. Chem Eng J. 2025;523(3):168471. doi:10.1016/j.cej.2025.168471.
18. Long SJ, Song JY, Luo Q, Zhao B, Zhang J, Zhang X, et al. *In situ* construction of iron-rich metal-organic frameworks on wool surface for enhanced flame retardancy and low smoke generation. Colloids Surf A Physicochem Eng Aspects. 2024;692:134034. doi:10.1016/j.colsurfa.2024.134034.
19. Qi M, Xin C, Han L, Liu W, Kirillov AM, Dou W, et al. Dual-functional La/Zn-MOF@Methylphosphonate composites: innovating high-performance flame retardancy and thermal stability of epoxy resin. React Funct Polym. 2025;215:106379. doi:10.1016/j.reactfunctpolym.2025.106379.
20. Cheng F, Zhu X, Yun F, Wei M, Shi C, Han J. *In-situ* construction of BiOCl@Cu-MOF for synergistic flame retardancy, smoke suppression, and antibacterial properties in PVC coatings. Prog Org Coat. 2025;208:109504. doi:10.1016/j.porgcoat.2025.109504.
21. Zhang F, Li X, Yang L, Zhang Y, Zhang M. A Mo-based metal-organic framework toward improving flame retardancy and smoke suppression of epoxy resin. Polym Adv Technol. 2021;32(8):3266–77. doi:10.1002/pat.5338.
22. Wei S, Zhong W, Xu P, Niu D, Yang W, Shen Y, et al. Synergistic effect of Co-MOF/epoxy modified tannic acid/ammonium polyphosphate on flame retardancy, anti-melt dripping and mechanical properties of polylactic acid. Chem Eng J. 2024;500:156772. doi:10.1016/j.cej.2024.156772.
23. Li C, Ba Z, Wu B, Shi X, Liu H, Ma L, et al. Bio-inspired construction of hydrophobic $Mg(OH)_2$/Co-MOF/DOPO hybrids for simultaneously improving flame retardancy and mechanical properties of poly(L-lactic acid) composites. Chem Eng J. 2025;504:158853. doi:10.1016/j.cej.2024.158853.
24. Li K, Zhang X, Li X, Chang Q, Deng S, Zhu G. Controllable adjustment of loading capacity of Cu-Zr bimetallic MOF on wood substrate to promote flame retardancy. J Therm Anal Calorim. 2025;150(7):4995–5006. doi:10.1007/s10973-025-14104-z.
25. Lu X, Lee AF, Gu X. Improving the flame retardancy of sustainable lignin-based epoxy resins using phosphorus/nitrogen treated cobalt metal-organic frameworks. Mater Today Chem. 2022;26:101184. doi:10.1016/j.mtchem.2022.101184.
26. Nie S, Zhao Z, Zhai W, Yang J, Zhang H, Zhao D, et al. Interfacial property optimization through the co-deployment of MOF-derived nickel phyllosilicate and DOPO: effective reinforcement and flame retardancy of epoxy resin. Compos Part B Eng. 2025;289(4):111947. doi:10.1016/j.compositesb.2024.111947.
27. Huang Y, He J, Yang R. Preparation and characterization of HNTs@ZIF enhanced intrinsic flame retardant RTV silicone rubber. Polym Degrad Stab. 2024;230:111036. doi:10.1016/j.polymdegradstab.2024.111036.

28. Tu Z, Ou H, Ran Y, Xue H, Zhu F. Heterogeneous ZIF-67@MMT with catalytic effect inhibits CO release: application of mismatch engineering design based on lotus leaf inspiration in flame retardant and toughening of polypropylene. Mater Today Commun. 2025;46:112829. doi:10.1016/j.mtcomm.2025.112829.
29. Wang H, Li X, Su F, Xie J, Xin Y, Zhang W, et al. Core-shell ZIF67@ZIF8 modified with phytic acid as an effective flame retardant for improving the fire safety of epoxy resins. ACS Omega. 2022;7(25):21664–74. doi:10.1021/acsomega.2c01545.
30. Song X, Li Q, Han Z, Hou B, Pan YT, Geng Z, et al. Synchronous modification of ZIF-67 with cyclomatrix polyphosphazene coating for efficient flame retardancy and mechanical reinforcement of epoxy resin. J Colloid Interface Sci. 2024;667(46):223–36. doi:10.1016/j.jcis.2024.04.088.
31. Wang X, Liu C, Meng D, Sun J, Fei B, Li H, et al. Surface integration of polyelectrolyte and zeolitic imidazolate framework-67 for multifunctional poly(lactic acid) non-woven fabrics. Appl Surf Sci. 2021;569:151039. doi:10.1016/j.apsusc.2021.151039.
32. Zhou J, Dong F, Liu C, Lu K. P, N, Si synergistic flame-retarding water polyurethane coating with superior flame retardancy and hydrophobicity. J Polym Res. 2023;30(7):260. doi:10.1007/s10965-023-03635-4.
33. Liang B, Liu K, Dai J, Chen W, Lu W. Polymer-type flame retardants based on a DOPO derivative for improving the flame retardancy of polyamide 6: preparation, properties and flame retardancy mode of action. Polym Degrad Stab. 2024;225:110807. doi:10.1016/j.polymdegradstab.2024.110807.